Ecosystem fluxes of carbonyl sulfide in an old-growth forest: temporal dynamics and responses to diffuse radiation and heat waves

Bharat Rastogi[1], Max Berkelhammer[2], Sonia Wharton[3], Mary E Whelan[4] Frederick C. Meinzer[5], David Noone[6], and Christopher J. Still[1]

[1] Department of Forest Ecosystems and Society, Oregon State University, OR 97331, USA
[2] Department of Earth and Environmental Sciences, University of Illinois at Chicago, Chicago, Illinois, USA
[3] Atmospheric, Earth and Energy Division, Lawrence Livermore National Laboratory, 7000 East Avenue, L-103, Livermore, CA 94550, USA
[4] Carnegie Institution for Science, 260 Panama St., Stanford, CA, USA, 94305

[5] USDA Forest Service, PNW Research Station, Corvallis, OR 97331, USA

[6] College of Earth, Ocean and Atmospheric Sciences, Oregon State University, OR 97331, USA

Corresponding author: Bharat Rastogi (bharat.rastogi@oregonstate.edu)

Abstract

Carbonyl sulfide (OCS) has recently emerged as a tracer for terrestrial carbon uptake. While physiological studies relating OCS fluxes to leaf stomatal dynamics have been established at leaf and branch scales and incorporated in global carbon cycle models, the quantity of data from ecosystem-scale field studies remains limited. In this study, we employ established theoretical relationships to infer ecosystem-scale plant OCS uptake from mixing ratio measurements. OCS fluxes showed a pronounced diurnal cycle, with maximum uptake during mid-day. OCS uptake was found to scale with independent measurements of CO_2 fluxes over a 60-m-tall old-growth forest in the Pacific Northwestern U.S. (45°49′13.76″ N; 121°57′06.88″) at daily and monthly timescales under mid-high light conditions across the growing season in 2015. OCS fluxes tracked changes in soil moisture, and were strongly influenced by the fraction of downwelling diffuse light. Finally, we examine the effect of sequential heatwaves on fluxes of OCS, CO_2 and H_2O. Our results bolster previous evidence that ecosystem OCS uptake is strongly related to stomatal dynamics, and measuring this gas improves constraints on estimating photosynthetic rates at the ecosystem scale.

1. Introduction

Carbonyl Sulfide (OCS) is the most abundant sulfur gas in the atmosphere, with a mean atmospheric concentration of ~500 ppt (parts per trillion), and therefore a significant part of the tropospheric and stratospheric sulfur cycles, with implications for the global radiation budget and ozone depletion (Johnson et al.,1993; Notholt et al., 2003). The dominant sink of atmospheric OCS is vegetation (Kesselmeier and Merk, 1993; Kettle et al., 2002; Montzka et al., 2007 and references therein), through rapid and irreversible hydrolysis by the ubiquitous enzyme carbonic anhydrase (Protoschill-Krebs, Wilhelm, &

Kesselmeier, 1996; Protoschill-Krebs and Kesselmeier, 1992). Recent advances in spectroscopic technology have enabled continuous in-situ measurements of OCS on timescales that are relevant to understanding stomatal function at the leaf-scale (Stimler et al., 2010a, 2010b), branch scale (Berkelhammer et al., 2014) and the ecosystem scale (Kooijmans et al., 2017; Wehr et al., 2017). An important distinction between OCS and CO_2 cycling is the absence of a retroflux from actively photosynthesizing leaves (OCS emissions have been reported from stressed crops following severe fungal infection; Bloem et al., 2012). However, the normalized leaf uptake ratio of OCS:CO_2 (LRU; Sandoval-Soto et al., 2005) is relatively constant at medium to high light levels (Maseyk et al., 2014; Stimler et al., 2010), making it an excellent proxy for quantifying plant productivity (GPP; Asaf et al., 2013; Billesbach et al., 2014; Blonquist et al., 2011). On the other hand, both uptake and emissions of OCS from soils have been identified (Whelan et al., 2016; Sun et al., 2015; Maseyk et al., 2014; Kesselmier et al., 1999). While ecosystem-scale measurements of OCS continue to establish links between OCS uptake and GPP in different ecosystems (for a comprehensive list of ecosystem scale studies readers are referred to Figure 2 in Whelan et al., 2017), inconsistencies persist. For example, in an oak-savanna woodland in southern France Belviso et al. (2016) found that OCS exchange was strongly influenced by photosynthesis during early morning hours, while meaningful values of LRU could only by calculated for a few days in the early afternoons. Commane et al. (2015) were unable to explain mid-summer emissions of OCS at a mid-latitude deciduous forest. Uncertainties highlighted above argue for field-scale measurements of OCS in a variety of ecosystems, particularly as OCS flux predictions have recently been incorporated to inform estimates of plant productivity in global carbon cycle models (Campbell et al., 2017a; Hilton et al., 2017; Launois et al., 2015).

OCS fluxes have not been previously reported for old-growth forests, although a recent study using flask samples inferred large uptake of OCS in coastal redwood forests in northern California (Campbell et al., 2017b). Rastogi et al. (in revision) found large drawdowns in mixing ratios of OCS at an old growth forest in the pacific northwestern U.S., and significant uptake of this gas by various components of the ecosystem (leaves, soils, and epiphytes). In this study, we report estimates of OCS fluxes from an old-growth forest and place them in the context of ecosystem carbon and water cycling. Additionally, we investigate the response of CO_2, H_2O and OCS fluxes to changes in the fraction of downwelling diffuse radiation, as well as heat wave events through the growing season. Technological constraints posed limitations in measuring fast-response OCS fluxes so instead we combine continuous in-situ measurements of OCS mixing ratios above and within the canopy with established theoretical equations for OCS uptake (see Berry et al., 2013; Commane et al., 2015; Seibt et al., 2010) to characterize OCS fluxes using a simple empirical model and compare them with ecosystem uptake of CO_2 from co-located eddy covariance measurements.

2. Methods

2.1. Site Description

Measurements were made at the Wind River Experimental Forest (WR), located within the Gifford Pinchot National Forest in southwest Washington state, USA (45°49′13.76″

N; 121°57′06.88″; 371 m above sea level). The site is well studied and described in great detail (Paw U et al., 2004; Shaw et al., 2004; Wharton and Falk, 2016; Winner et al., 2004). The climate is classified as temperate oceanic with a strong summer drought. The forest is 478 ha of preserved old-growth evergreen needle-leaf forest, with dominant tree species of Douglas fir (*Pseudotsuga menziesii*) and Western hemlock (*Tsuga heterophylla*). The tallest Douglas fir trees are between 50 and 60m, while the shade-tolerant hemlocks are typically between 20-30 m high. Maximum rooting depth is 1–2 m for the tallest, dominant Douglas-fir trees although most of the root biomass is concentrated in the first 0.5 m (Shaw et al., 2014). The cumulative LAI is estimated to be 8-9 $m^2 m^{-2}$ (Parker et al., 2004). Additionally, the ecosystem hosts a large diversity of mosses, lichens and other epiphytic plants, which play an important role in canopy OCS dynamics (Rastogi et al., in revision). The soils are volcanic in origin, although most of the forest surface is comprised of decaying organic matter (Shaw et al., 2004).

2.2. Study period: Measurements reported here are between April 18- Dec 31, 2015. However, in early November an intake line at the top of the canopy was damaged after a rainstorm. Measurements continued at the other intake heights (see sections 2.4 and 2.9). Therefore, ecosystem fluxes and related analyses in this study cover 136 days between April 18 and October 31, while chamber based soil fluxes are reported for the months of August-December. Gaps in the time series due to analyzer maintenance correspond to Jun 26-28, July 6-17, August 4-7, August 24 and October 4-7. April-October roughly corresponds to most of the growing season, although at this site GPP usually peaks early in March-April, when soil moisture is high and ecosystem respiration flux is low, while plant productivity is typically severely light and temperature limited in the months of November-December (Wharton and Falk, 2016). Environmental conditions during the measurement campaign are shown in Figure 1 are represent a typical Mediterranean-type climate, with temperature peaking in July and minimal to no measured rainfall between June and September. This results in high summertime atmospheric vapor pressure deficit (VPDa), and soil moisture declines steadily through the summer period, with some recharge following rare precipitation events in September and then more commonly in October. The measurement period also encompasses three distinct heat waves, characterized by anomalously high air temperatures and mid-day VPDa values (often exceeding 4 kPa). We examine the response of OCS and CO_2 fluxes during these heat waves.

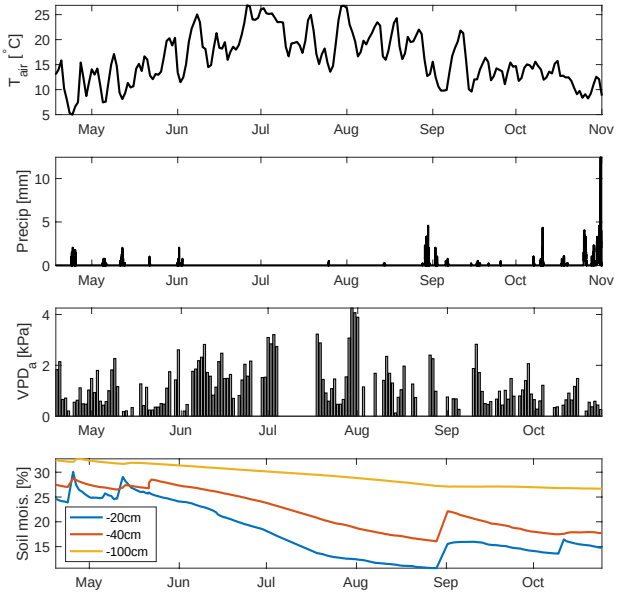

Figure 1. Environmental conditions at Wind River during the measurement campaign. daily mean air temperature (a), precipitation (b) mid-day VPDa (c) and soil moisture measured at three depths (d) are shown.

2.3. CO_2 and H_2O eddy flux measurements: Carbon, water and energy fluxes have been collected since 1998 at the Wind River AmeriFlux tower (US-wrc; Paw U et al. 2004). For further details readers are referred to Falk et al., (2008; instrumentation and data processing), and Wharton et al., (2012) and Wharton and Falk, (2016) for multi-year carbon and water flux measurements and synthesis.

2.4. OCS measurements: A commercially available off-axis integrated cavity output spectroscopy analyzer manufactured by Los Gatos Research Inc., (LGR; model 914-0028) was deployed at the base of the tower in an insulated and temperature-controlled shed. The instrument measures mixing ratios of OCS, CO_2, H_2O and CO simultaneously at a maximal scan rate of 5Hz. The system uses a 4.87 μm cascade laser coupled to a high finesse 800 cm^3 optical cavity and light transmitted through the cavity is focused into a cooled and amplified HgCdTe detector. OCS is detected at ~2050.40 cm^{-1}, CO_2 at 2050.56 cm^{-1}, CO at ~2050.86 cm^{-1}, and H_2O at ~2050.66 cm^{-1}. Pressure broadening associated with changes in the concentration of water vapor in the samples is corrected for in the analysis routine. Air was sampled through 0.25'' diameter PFA tubing using a diaphragm pump at a flow rate of 2L min^{-1}, from inlets located at 70m (at the height of the eddy flux instrumentation), 60m (canopy top), 20m, 10m, and 1m. The sampling frequency was 0.1Hz and the sampling interval was 5 minutes. The first minute of each sampling interval was removed to avoid any inter-sampling mixing. The remaining data were checked for temperature and pressure fluctuations inside the measurement chamber, and a moving window filter was used to eliminate any sudden outliers in the data. Mixing ratios were aggregated to provide hourly means. For detailed information regarding instrumentation and the measurement readers are referred to Rastogi et al (in revision), Berkelhammer et al. (2014) and Belviso et al. (2016).

2.5. Calibration: Calibration was performed using ambient air stored in insulated tanks as a secondary reference. Air was sampled into the analyzer daily, and tank pressure was routinely monitored to check for leaks. Glass flasks were randomly sampled from calibration tanks and measured against a NOAA GMD reference standard. Cross-referencing revealed that the accuracy of the measurement was within the reported minimum uncertainty of the instrument (of 12.6 pmol mol^{-1}; Berkelhammer et al., 2016).

2.6. Thermal Camera measurements: Leaf temperatures were measured from October 28, 2014 to January 28, 2016 using a FLIR A325sc thermal camera (FLIR System Inc., Wilsonville, OR), in which a FLIR IR 30-mm lens (focal length: 30.38 mm; field of view: 15°×11.25°) was installed. The thermal camera has a pixel resolution of 320 × 240. Within the field of view (FOV), spot sizes of a single pixel are 0.83 cm from 10-m distance and 8.3 cm from 100-m distance. Manufacturer-reported errors in original measured thermal temperatures are ±2 °C or ±2% of the measurements. The camera model is identical to one used in another study at an AmeriFlux site in central Oregon (US Me-2), and the detailed specifications can be found in Kim et al. (2016). To monitor a larger canopy region, a pan-tilt unit (PTU) was used for motion control, allowing multiple canopy thermal image acquisition within one motion cycle. We used a FLIR PTU-D100E (FLIR System Inc., Wilsonville, OR; (http://www.flir.com/mcs) to move the thermal camera vertically and horizontally at specific pan and tilt angles. We selected five pan-tilt angle (PT) positions representing the upper canopy (i.e., ~40 to 60 m above the forest floor) to estimate leaf temperatures in this study.

2.7. Diffuse light measurement and analyses: An SPN1 Sunshine Pyranometer (Delta-T Devices ltd., Cambridge, U.K.) was installed at the top of the canopy and collected direct and diffuse shortwave downwelling radiation from April- December 2015. Measurements were made every 1 min, and then aggregated to hourly means. We limited our analyses of diffuse radiation data to include only mid-day hours (between 11am-1pm) to minimize the influence of solar angles on diffuse radiation fractions. We defined three distinct periods based on the ratio of diffuse radiation to total incoming solar radiation (*fidff*). Data were characterized as clear if *fdiff* < 0.2; partly cloudy if *fdiff* > 0.2 and *fdiff* < 0.8, and overcast if *fdiff* > 0.8.

2.8. OCS flux estimation: 'Canopy-scale leaf' OCS flux was estimated using flux-gradient similarity, following Commane et al., 2015.

$$F_{OCS} = F_{H2O} \cdot \frac{g_{OCS}}{g_{H2O}} \quad (1)$$

where F_{OCS}, F_{H2O}, g_{OCS} and g_{H2O} are the fluxes and gradients of OCS and H_2O, respectively. Following Seibt et al., (2010) and Berry et al., (2013), we assume that OCS is irreversibly and rapidly consumed inside leaves, such that the gradient between ambient air and the leaf interior effectively reduces to the ambient measured OCS mixing ratio:

$$g_{OCS} = \chi^a_{OCS} - \chi^l_{OCS} = \chi^a_{OCS} \quad , \quad (2)$$

where g_{OCS} is defined as he gradient of OCS between ambient air and the leaf intercellular spaces (χ is the mixing ratio of OCS and superscripts *a* and *l* refer to ambient

and leaf respectively). In our study, χ^a_{OCS} is the measured mixing ratio at the canopy top (60m) instead of above canopy (70m) to account for turbulent transport between the canopy top and air that is above the canopy top. We use vapor pressure deficit (VPD) as the corresponding gradient for H_2O, under the key assumption that the intercellular leaf surfaces are saturated with water vapor. While VPD is usually calculated using air temperature, a more accurate calculation can be performed with leaf temperatures, which can deviate significantly from air temperatures (Kim et al. 2016), leading to significant differences between the VPD of ambient air and that at the leaf surface (Fig. 2a and 3d in this study). Previously leaf temperatures have been inferred from sensible heat fluxes, wind speed and air temperatures (e.g. Wehr et al., 2017), here we use explicit measurements of leaf skin temperatures to estimate leaf-air VPD ($VPD_{l.}$). Analogous to Eq (3),

$$g_{H2O} = \chi^l_{H2O} - \chi^a_{H2O} = \frac{(e_i - e_a)}{P} = \frac{VPD_l}{P} \quad , \tag{3}$$

where e_i is saturation vapor pressure in the leaf sub-stomatal cavity (kPa), using leaf skin temperature, ea is the actual vapor pressure (kPa), P is the measured atmospheric pressure (kPa) at the tower top, and $\chi^l_{H_2O}$ and $\chi^a_{H_2O}$ (ppth) are the leaf and ambient H_2O mixing ratios at the canopy top. Finally, since gradients of OCS and H_2O are estimated between ambient air and the leaf intercellular spaces, these are normalized by the ratio of diffusivities of these two species in air (Seibt et al., 2010; Wohlfahrt et al., 2012).

F_{H2O} was measured using eddy covariance at the tower top (70m). In high LAI forests with minimal exposed soil, such as those of the Pacific Northwest, fluxes of F_{H2O} can be treated as a good proxy for transpiration, since soil evaporation should be minimal. We excluded rainy days, as well as two days following rainfall, to only capture periods when F_{H2O} can be assumed to be dominated by transpiration. Equation (1) was evaluated only under the condition $F_{H2O} > 0.2$ mmolm^{-2}s^{-1}. We restricted our analyses to daytime, when OCS flux is assumed to be related to leaf CO_2 uptake (Maseyk et al., 2014; Wehr et al., 2017).

Leaf Relative uptake was calculated following Seibt et al (2010).

$$LRU = \frac{F_{OCS}}{GPP} . \frac{\chi CO_2}{\chi OCS} \quad , \tag{5}$$

where GPP was estimated from CO_2 fluxes measured at the tower top, using a nighttime based partitioning approach (Reichstein et al., 2005), that was optimized for the site (Falk et al., 2008). Finally, canopy conductance (Gc) was estimated using a simple flux-gradient approach with the assumption that the canopy (or ecosystem) acts as a single big leaf.

$$Gc = F_{H2O} . \frac{VPD_l}{P} \quad , \tag{6}$$

2.9. Surface Fluxes: A long-term automatic soil survey chamber (Li-Cor 8100-104, 20 cm diameter) was installed at three 0.03 m^2 surface sites in series, within 1 meter of each other. All plastic and rubber parts had been removed from the chamber and replaced with materials compatible with OCS measurements: stainless steel, PFA plastic, and Volara

foam. Blank measurements were performed in the laboratory before deployment and OCS concentrations in the chamber were found to be statistically indistinguishable from incoming ambient concentrations. The stainless-steel chamber top opened and closed automatically on a timer. Gas was drawn through the chamber via a pump downstream of the analyzer, and the 3 $Lmin^{-1}$ flow rate was confirmed with a mass flow meter. When the chamber was open, ambient near-surface air was observed. When the chamber was closed, trace gas concentrations reached a stable state for at least 2 minutes during the 10-minute incubation time. The difference between the ambient concentration and the stable closed-chamber concentration were used to calculate the surface fluxes of OCS and CO_2.

$$F_{forest\ floor} = M_c \Delta\chi . A^{-1} , \quad (7)$$

where M_c is the measured flow rate into the chamber (converted from $Lmin^{-1}$ to $mols^{-1}$ using the ideal gas law) and $\Delta\chi$ is the difference between mixing ratios of OCS or CO_2 in ambient air and the chamber and A is the surface area of the chamber. The minimum flux detectable with this method was 1.2 $pmolm^{-2}s^{-1}$ uptake or production.

Care was taken to select sites characteristic of the surface, which was generally springy and covered in a mat of mosses and lichen. Surface flux observations were made at site 1 from July 6 to 16, site 2 from August 13 to October 7, and site 3 from November 6 to December 2, 2015. The first site was visually similar to the subsequent two sites at the surface, though the chamber base of the first site was installed into the moss layer and a barely decomposed fallen tree. When a soil sample was attempted to be extracted from the footprint of the chamber base, several liters of intact wood litter were removed. The influence of the developed soil on site 1 is therefore considered minimal. Site 2 was selected nearby and observations were made until a dominant tree fell on the soil chamber. The chamber was repaired and re-installed a month later at site 3 and observations continued without incident until the chamber was removed in advance of the soil freezing.

3. Results and Discussion:

3.1. Ecosystem fluxes: The composite diurnal cycles for CO_2, water vapor and OCS and fluxes are shown (Fig. 2a-c). The total ecosystem flux of OCS (F_{OCS}; Fig 2.b.) follows a pronounced diurnal cycle that peaks during daylight hours. The vertical profile of mixing ratios measured throughout the canopy is also shown (right y-axis and orange lines in Fig.2.b). OCS mixing ratios are highest at the canopy top and lowest near the forest floor, but mixing ratios increase from the early morning to mid-afternoon. Together these processes are indicative of ecosystem uptake and downward entrainment of boundary layer air. While entrainment helps explain the diurnal cycle of observed mixing ratios, this flux integrates to zero at daily and longer time scales (Rastogi et al., in revision). The shape of the F_{OCS} curve is very similar to those of net and gross carbon fluxes (Fig 2.b-c), although F_{OCS} was consistently negative throughout the 24-hour period, implying ecosystem uptake during nighttime and daylight hours. While nighttime uptake of OCS (mean nighttime flux ~ -10 ± 1 $pmolm^2s^{-1}$) is likely due to a combination of soil, epiphyte, and vascular plant uptake due from partially closed stomata, daytime uptake is likely dominated by vascular plant stomatal activity. Leaf relative uptake, a ratio of F_{OCS}:GPP normalized by the mean mixing ratios of OCS:CO_2, showed a strong light

dependence. High-light, mid-day values ranged between 3-4, which is higher than those observed at other forest systems (Kooijmans et al., 2017; Wehr et al., 2017) but well within the spread of values obtained in a recent meta-analyses of OCS studies for vegetated ecosystems (Whelan et al., 2018). The diurnal cycle was found to be asymmetric, with peak values observed in the early morning, when stomatal conductance is likely to be high (Winner et al., 2004), but GPP is limited by low light levels. It is important to note that LRU is likely influenced by large amounts of epiphyte and understory vegetation, which assimilate OCS even at times when ecosystem CO_2 uptake is low or zero. Epiphytic assimilation of OCS is highly influenced by moisture content (Gimeno et al., 2017) and is typically higher through the night and in the early mornings at this site (Rastogi et al., in revision). Moreover, in tall old-growth forests, leaf area is vertically distributed over a much larger part of the canopy compared to other forests (Parker et al., 2004). While leaves at the canopy top exercise tight stomatal control to limit water loss and minimize hydraulic failure (Woodruff et al., 2007) leaves lower down in the canopy, including those of understory vegetation, likely impose less stomatal control of transpiration (Winner et al., 2004). Lower-canopy leaves may therefore continue to disproportionately assimilate OCS, even under low rates of carbon assimilation (as CO_2 uptake is additionally light limited).

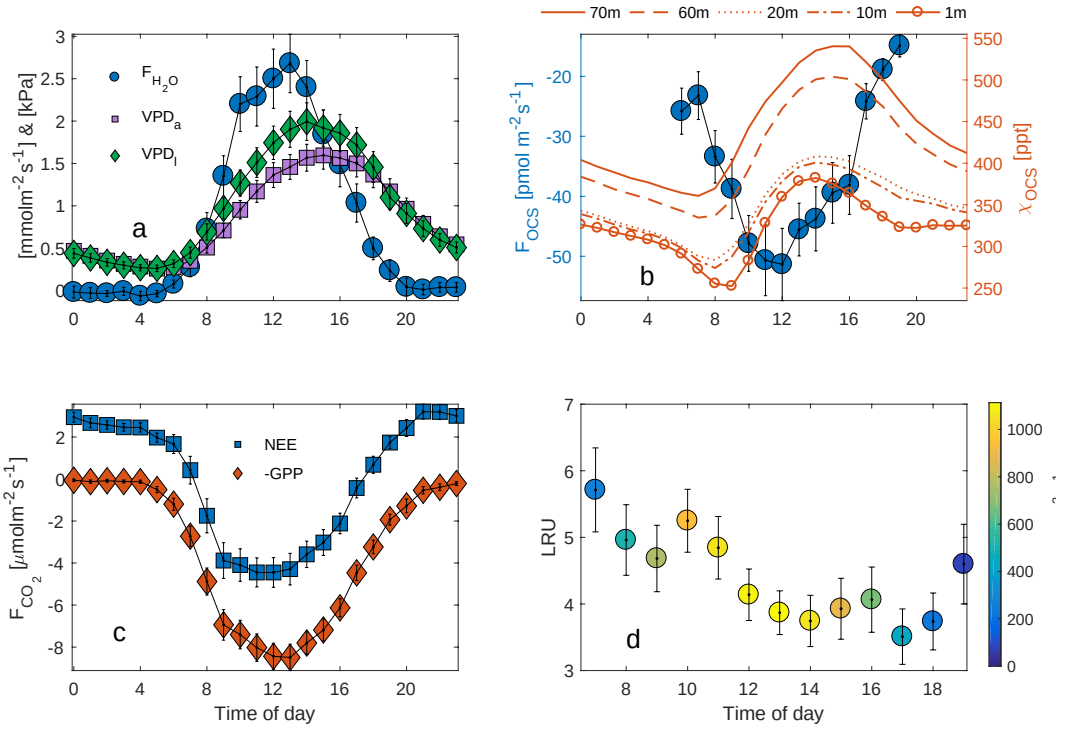

Figure 2. Diurnal cycle of H_2O flux (blue circles) and VPD estimated from air and leaf temperatures (purple squares and green diamonds respectively; a), estimated OCS flux (circles, left axis) and mixing ratio profile (right axis; b), NEE and GPP (blue squares and red diamonds; c), and leaf relative uptake (calculated only during daylight hours, colors represent Photosynthetically active radiation; d). Vertical bars indicate standard error.

3.2. Daily and seasonal dynamics: Daytime fluxes of OCS were correlated to independent estimates of GPP (Fig. 3a), and uptake of both OCS and CO_2 reduced as soil moisture declined. Variability in the relationship between fluxes of OCS and CO_2 and soil moisture was related to VPD, which fluctuated as a response of changing cloud cover (discussed later in sec. 3.4).

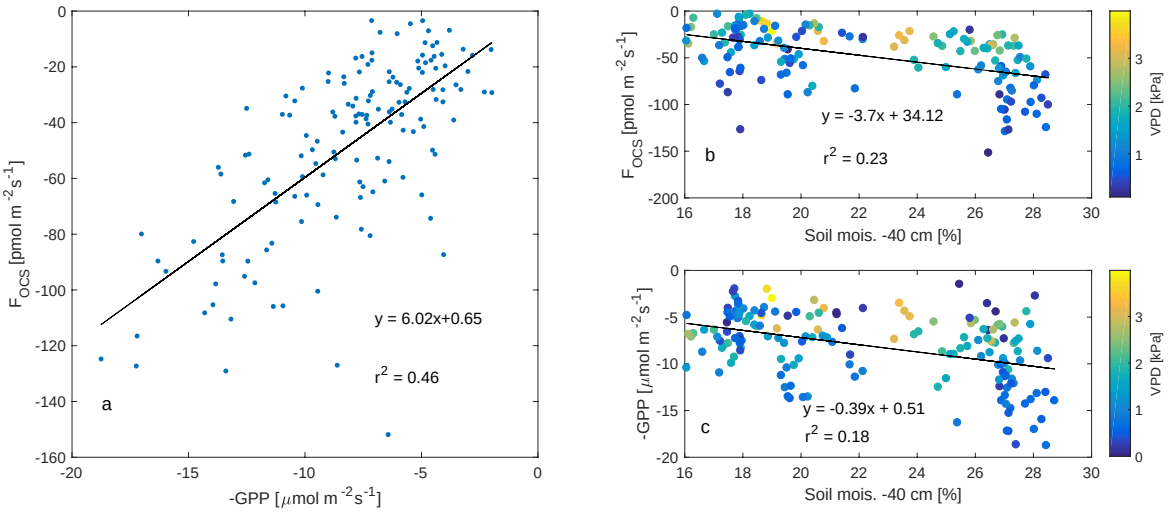

Figure 3. F_{OCS} was linearly correlated to GPP (plotted as a negative quantity to show ecosystem uptake; a), while both FOCS and GPP reduced as a function of decreasing soil moisture (b-c). Data presented here are mid-day means, data in (b-c) are colored according to VPD.

Ecosystem uptake of OCS and CO_2 (as well as GPP) was highest in April (Fig. 4a), and declined as the soil drought progressed (Fig. 4f). Mean monthly maximum OCS flux was estimated as -61 ± 6 $pmolm^{-2}s^{-1}$, while daily mean maximum GPP over this period was estimated as 10 ± 1$\mu molm^{-2}s^{-1}$ (plotted as a negative quantity in Fig. 4b to show ecosystem uptake). While the steepest declines in F_{OCS}, NEE and GPP happened between the months of May and June, F_{OCS} continued to decline through the rest of the summer, with a minimum in August, and remaining low in September and October. CO_2 fluxes flattened between June-September, before declining again in October. While uptake of OCS and CO2 followed similar patterns, H_2O flux remained high until mid-summer (Fig. 4c) before plunging in August, presumably due to a combination of high VPD (Fig. 4d) and declining soil moisture (Fig. 4f), as plants exercised greater control over stomata. This can be clearly seen in the seasonal cycle of canopy conductance (Gc; Fig. 4e). Mean monthly Gc was highest in the months of April and May, and then declined in response to increasing VPD and decreasing soil moisture, before increasing again slightly in September and October following soil recharge and decreased VPD due to precipitation events. In October, soil water recharge, several rain-free days (Fig. 1), and lower VPD (Fig. 4d) do not result in increased gas exchange, likely due to downregulation of photosynthesis (Eastman and Camm, 1995), induced by photoprotective changes in the xanthophyll cycle (Adams and Demmig-Adams, 1994).

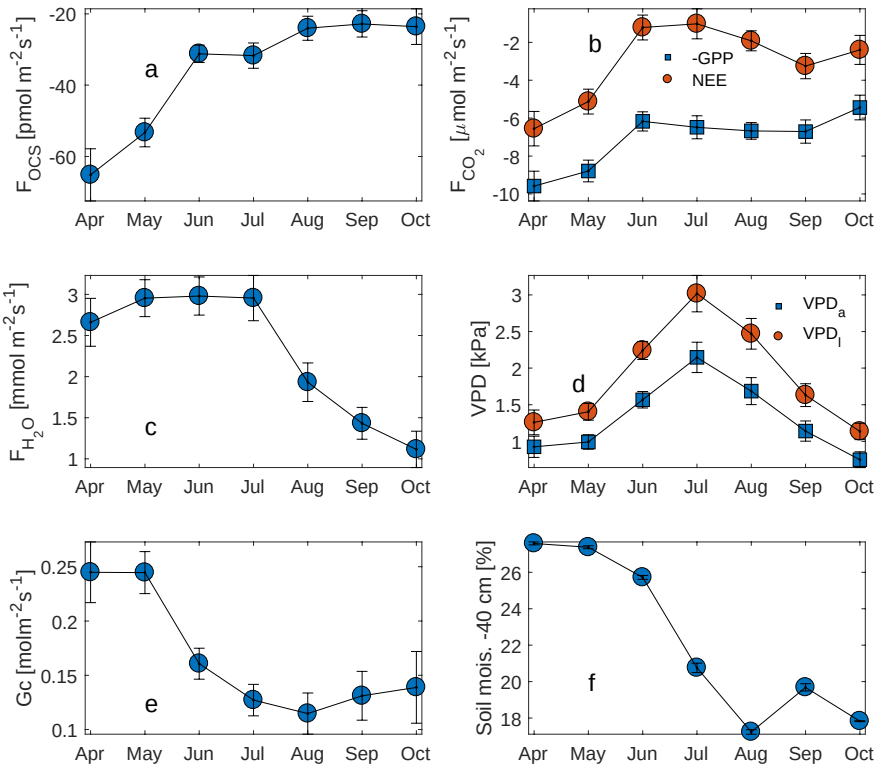

Figure 4. Monthly means for daytime F_{OCS}, NEE and -GPP (red circles and blue squares; b), water vapor flux (c), VPD_a and VPD_l (blue squares and red circles; d), canopy conductance (Gc; e), and soil moisture at -40cm depth (f). Vertical bars indicate standard error.

3.3. Surface Fluxes: Forest floor OCS fluxes were observed from 3 sites in series and within 1 m of each other. Site 1 had approximately twice the OCS uptake compared to the subsequent two sites and had a substantial layer of intact woody debris under the chamber footprint. Site 2 and 3 had OCS fluxes similar to previous surface fluxes reported for forests (Whelan et al., 2018). For all sites, there was no clear diurnal pattern. For site 2, uptake immediately following chamber installation was higher (~6 pmol $m^{-2}s^{-1}$) than fluxes later on (all <6 pmol $m^{-2}s^{-1}$) when temperatures were lower (Fig 5). Site 3 did not have high uptake after chamber installation, and had consistent fluxes between the detection limit and -6.2 pmol $m^{-2}s^{-1}$ for the first few weeks. When ambient air temperatures dropped below freezing, uptake remained unchanged, except for the largest uptake observed (6 to 12 pmol $m^{-2}s^{-1}$) during two events when average air temperature fluctuated from a cooling to warming trend. Soil temperature never dropped below freezing during the experiment and was generally colder over time. We did not observe any OCS emissions from the chamber based measurements, consistent with recent studies that find that cooler, moist (Maseyk et al., 2014; Sun et al., 2016; Whelan et al., 2016) and radiation limited (Kitz et al., 2017) soils do not emit OCS.

Surface CO_2 emissions exhibited a relationship with temperature, where highest production (~25 µmol $m^{-2}s^{-1}$) corresponded with temperatures ~15°C, and maximum flux values decreased for warmer and colder temperatures. CO_2 emissions had a diurnal

pattern, with lowest emissions at night and maximum emissions in late morning to mid-afternoon. No obvious relationship emerges from CO_2 emission and OCS uptake, though the high OCS uptake events in late November and early December have a linear relationship with CO_2 emissions. For sites 2 and 3, the ratio of OCS emission to CO_2 production, normalized by the concentration of OCS and CO_2 in the closed chamber, was between -0.25 and -3.5 with a mean of -1. In contrast, the same ratio for site 1 varied from -5 to -19 with a mean of -10.

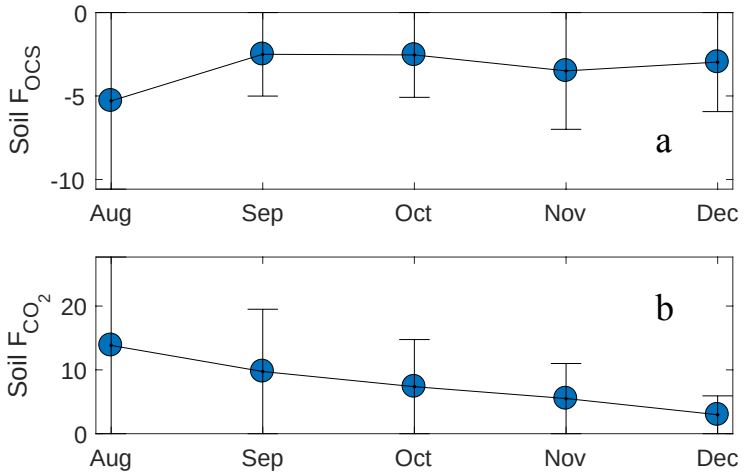

Figure 5. Surface F_{OCS} and F_{CO2} from chamber measurements (brown squares in a-b) from sites 2 and 3. Site 1 was atypical (see section 2.7) and therefore fluxes are not shown. Values for site 1 F_{OCS} and F_{CO2} were -22 ± 0.3 $pmolm^{-2}s^{-1}$ and -83 ± 2 $\mu molm^{-2}s^{-1}$ respectively. Error bars indicate standard deviation.

3.4. Sensitivity to diffuse light: Mid-day fluxes of OCS and CO_2 were found to be sensitive to changes in the fraction of diffused: total incoming shortwave radiation (*fdiff*; Figure 6b-c). For these analyses, data were separated into three periods corresponding to early summer (DOY 109-180), mid-late summer (DOY 180-240) and early fall (DOY 240-297), and binned into three categories: clear sky conditions, partly cloudy, and overcast, defined in sec. 2.7. Mid-day VPD was highest under clear sky conditions and lowest under overcast skies, but was most different across the three periods, during clear skies (Fig. 6a). Consequently, OCS and CO_2 uptake was highest (most negative fluxes) under overcast conditions during the early summer, and generally declined as *fdiff* decreased across all time periods (Fig. 6b-d). Across the three periods, the rate of decrease was much higher as *fdiff* changed from partially cloudy to clear. During the mid-late summer, however, (red diamonds in Fig. 6a-f), the diffuse light effect resulted in GPP and NEE being almost as high as during the early summer. F_{OCS} was also highest under partially cloudy skies during this time, and only showed a very weak decline under completely overcast conditions. Overall, the behavior of OCS and CO_2 fluxes was similar during the later time periods. Leaf relative uptake (LRU; calculated according to eq. 5) was lowest under partly clear skies and highest under overcast conditions. This is because under highly diffuse conditions, carbon uptake is additionally limited by light, whereas F_{OCS} is not (Wehr et al., 2017; Maseyk et al., 2014). The shape of the LRU curves can additionally be explained by examining canopy conductance (Gc; Fig. 6f), which was

also higher under overcast skies. LRU increased with Gc across all three periods (Fig. 6g), and appeared to be constant for Gc greater than ~400 mmolm^{-2}s^{-1}.

The diffuse light enhancement of stomatal and canopy conductance is well documented across a range of forest ecosystems (Alton et al., 2007; Cheng et al., 2015; Hollinger et al., 2017; Urban et al., 2007; Wharton et al., 2012). Lower VPD (Fig. 6a) and light levels allow plants to keep stomata open at mid-day and continue fixing CO_2. Lower VPD reduces transpirational losses, and the lack of VPD-induced partial stomatal closure reduces the resistance to CO_2 diffusion into the leaf. Correspondingly, the less directional nature of diffuse solar radiation allows greater penetration into the canopy, thus increasing photosynthesis across the entire canopy, even as a reduction in canopy top leaf photosynthesis is observed due to a reduction in total radiation. In a multi-year analysis at Wind River, Wharton et al., (2012) found that cloudy and partly cloudy sky conditions during the peak-growing season lead to an increase in CO_2 uptake. During our study, Gc was generally higher in the early growing season, but increased as sky conditions changed from clear skies to overcast. This increase was similar across the three time periods, even as the response of OCS and CO_2 fluxes was different across these periods. This indicates that declining soil moisture (Fig. 3b-c) likely limits gas exchange as the summer progresses, even as canopy conductance can be reasonably high under overcast skies.

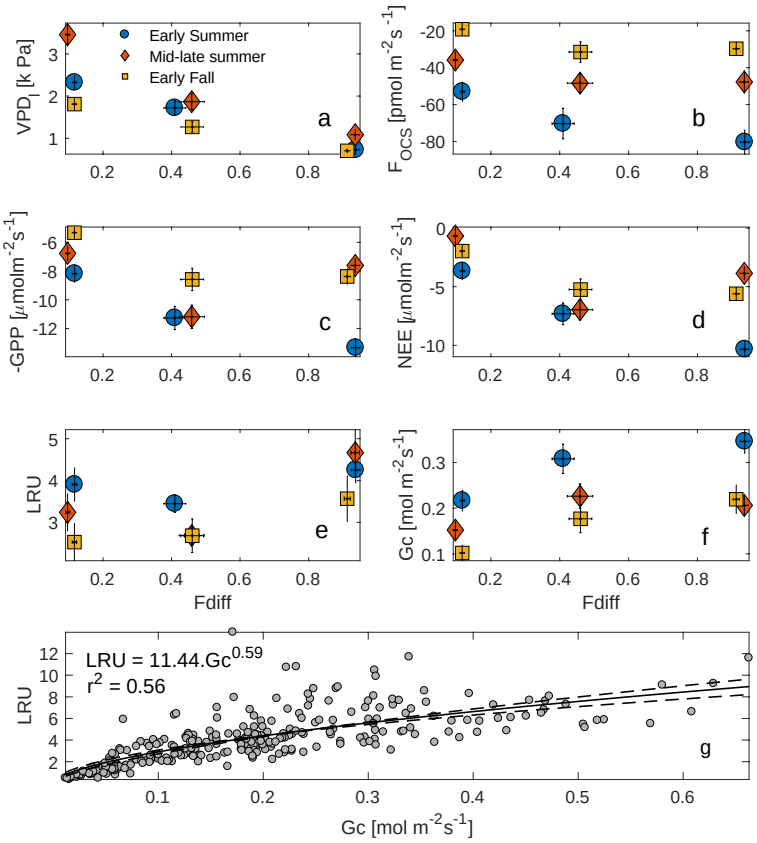

Figure 6. Mid-day VPDl, FOCS, NEE and GPP plotted against the fraction of diffuse downwelling shortwave radiation (a-d) for early summer, mid-late summer and early fall

of 2015 (these periods are defined in Section 3.4). High values on the x-axis indicate completely overcast or cloudy conditions, whereas as low values indicated clear skies. LRU increases with increasing *fdiff* during each period but the increase is most pronounced in the early summer (e). Gc increases from clear to partly cloudy conditions across the three periods and plateaus during overcast sky conditions (f). Vertical bars indicate 1 standard error. Across the three periods, LRU increased with Gc, and levelled off at Gc values greater than ~ 0.5 mol $m^{-2}s^{-1}$ (g).

3.5. Response to heat waves: 2015 was the warmest year in large parts of the Pacific Northwest since records began in the 1930s (Dalton et al., 2017). We observed three distinct heat waves during the 2015 summer. These were in early June (DOY 157-160), end of June- early July (DOY 175-188) and late July-early August (DOY 210-213). The three heat waves are shown as red, yellow and dark purple lines in Fig. 7; the overall time series is shown in blue (mid-day means are plotted for all variables). Mid-day temperatures exceeded 30°C during these heat wave events, while VPD-leaf exceeded 3 kPa during the first heat wave and increased to a maximum of 5.3 kPa during the last event (Fig. 7b). During the first event, F_{OCS} was similar to days immediately prior (Fig. 7c), but the canopy became a net source of CO_2 during all three events (Fig. 7d). The third events lead to a reduction in F_{OCS}, even though the canopy had received some rainfall in the preceding weeks (Fig. 1c). Water vapor fluxes (Fig. 7e) increased during the first heat wave, compared to days immediately prior. The increased water vapor flux is likely form an increase in transpiration under high VPD_l (red bars in Fig. 7b). Even as canopy conductance (Fig. 7f) is reduced under the third heatwave, high VPD_l ensures a steady transpirational flux (purple bars in Fig. 7e).

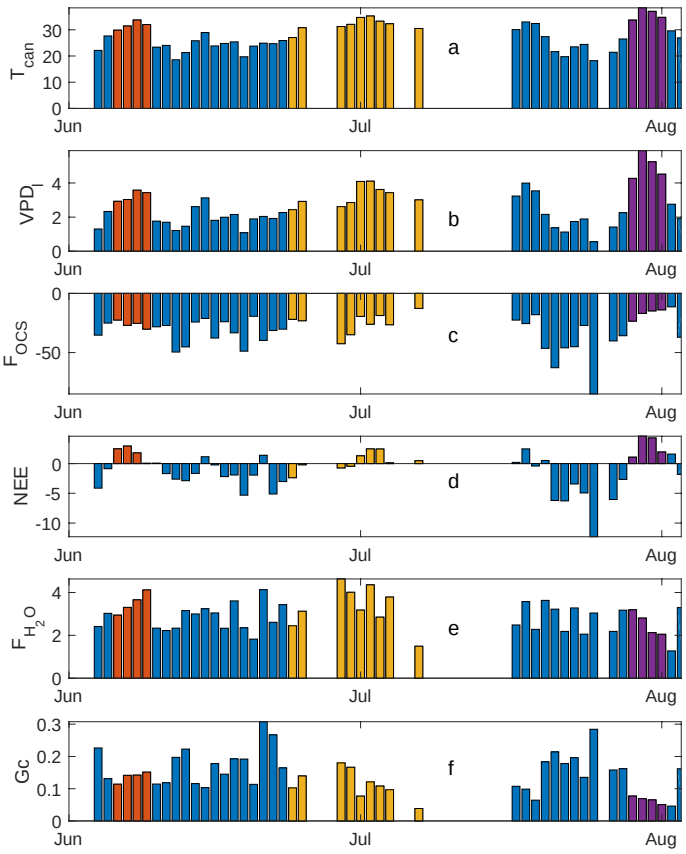

Figure 7. Mid-day means (11am-1pm local time) for three heat wave periods (plotted as red, yellow and purple, while the overall time series is shown in blue). Variables displayed are canopy temperature (°C; a), VPD-leaf (b), F_{OCS} (c), NEE (d), water vapor flux (e), and canopy conductance (Gc, f). Units for each panel are the same as specified in previous figures.

4. Conclusions

Over hourly, daily and seasonal timescales, estimates of F_{OCS} generally tracked fluctuations in GPP, implying stomatal control of carbon, water, and OCS fluxes at the site. We used continuous in-situ measurements of OCS mixing ratios, collocated measurements of water vapor fluxes, and air and canopy temperatures to calculate OCS uptake. We found the forest to be a large sink for OCS, with sink strength peaking during daylight hours. The mean LRU was ~ 4, and varied in response to changing light conditions and canopy conductance. These LRUs are larger than observed from other ecosystem scale studies, but well within the range of reported values (Whelan et al., 2018; Sandoval-Soto et al., 2005). The forest surface was found to be a soil moisture dependent sink of OCS. Ecosystem fluxes of OCS and CO_2 were found to be strongly sensitive to the ratio of diffuse: direct radiation reaching the top of the canopy. Uptake of both OCS and CO_2 increased as sky conditions changed from clear to partly cloudy. A much smaller increase in uptake was observed as sky conditions changed from partly cloudy to overcast, except during the early summer, when soil moisture was not limiting. This change was mediated by the sensitivity of stomata to changing cloudiness and soil

462 moisture, as estimated from canopy conductance. Finally, we examined the response of
463 OCS, CO_2 and H_2O fluxes on heatwaves, and found that sequential heatwaves lead to
464 suppression in stomatal gas exchange of all three fluxes.

465 Our results support the growing body of work that suggests ecosystem-scale OCS uptake
466 is controlled by stomatal dynamics. While moist old-growth forests in Pacific
467 Northwestern U.S. do not represent a very large fraction of the global terrestrial surface
468 area, results from this study are likely relevant for other old-growth forests, particularly
469 high LAI and very wet forests with extensive epiphyte cover, which are widespread in the
470 humid tropics.

471 Acknowledgements:

472 This work was partly funded by NASA SBIR Phase II award NNX12CD21P to LGR,
473 Inc. ("Ultrasensitive Analyzer for Realtime, In-Situ Airborne and Terrestrial
474 Measurements of OCS, CO2, and CO."). We would like to thank the US Forest Service
475 and the University of Washington for letting us use the research facility at Wind River. In
476 particular, we wish to sincerely acknowledge Ken Bible and Matt Schroeder for their help
477 with setting up the experiment as well as maintenance throughout the measurement
478 campaign. Data collected and used in this study can be accessed at
479 ftp.fsl.orst.edu/rastogib/Biogeosciences2018_Rastogi.

480 References:

481 Adams, W. W. and Demmig-Adams, B.: Carotenoid composition and down regulation of
482 photosystem II in three conifer species during the winter, Physiol. Plant., 92(3), 451–458,
483 doi:10.1111/j.1399-3054.1994.tb08835.x, 1994.

484 Alton, P. B., North, P. R. and Los, S. O.: The impact of diffuse sunlight on canopy light-
485 use efficiency, gross photosynthetic product and net ecosystem exchange in three forest
486 biomes, Glob. Chang. Biol., 13(4), 776–787, doi:10.1111/j.1365-2486.2007.01316.x,
487 2007.

488 Asaf, D., Rotenberg, E., Tatarinov, F., Dicken, U., Montzka, S. A. and Yakir, D.:
489 Ecosystem photosynthesis inferred from measurements of carbonyl sulphide flux, Nat.
490 Geosci., 6(3), 186–190, doi:10.1038/ngeo1730, 2013.

491 Belviso, S., Reiter, I. M., Loubet, B., Gros, V., Lathière, J., Montagne, D., Delmotte, M.,
492 Ramonet, M., Kalogridis, C., Lebegue, B., Bonnaire, N., Kazan, V., Gauquelin, T.,
493 Fernandez, C. and Genty, B.: A top-down approach of surface carbonyl sulfide exchange
494 by a Mediterranean oak forest ecosystem in Southern France, Atmos. Chem. Phys.
495 Discuss., (June 2012), 1–25, doi:10.5194/acp-2016-525, 2016.

496 Berkelhammer, M., Asaf, D., Still, C., Montzka, S., Noone, D., Gupta, M., Provencal, R.,
497 Chen, H. and Yakir, D.: Constraining surface carbon fluxes using in situ measurements of
498 carbonyl sulfide and carbon dioxide, Global Biogeochem. Cycles, 28(2), 161–179,
499 doi:10.1002/2013GB004644, 2014.

Berkelhammer, M., Steen-Larsen, H. C., Cosgrove, A., Peters, A. J., Johnson, R., Hayden, M. and Montzka, S. A.: Radiation and atmospheric circulation controls on carbonyl sulfide concentrations in themarine boundary layer, J. Geophys. Res., 121(21), 13,113-13,128, doi:10.1002/2016JD025437, 2016.

Berry, J., Wolf, A., Campbell, J. E., Baker, I., Blake, N., Blake, D., Denning, A. S., Kawa, S. R., Montzka, S. A., Seibt, U., Stimler, K., Yakir, D. and Zhu, Z.: A coupled model of the global cycles of carbonyl sulfide and CO_2: A possible new window on the carbon cycle, J. Geophys. Res. Biogeosciences, 118(2), 842–852, doi:10.1002/jgrg.20068, 2013.

Billesbach, D. P., Berry, J. A., Seibt, U., Maseyk, K., Torn, M. S., Fischer, M. L., Abu-Naser, M. and Campbell, J. E.: Growing season eddy covariance measurements of carbonyl sulfide and CO2 fluxes: COS and CO2 relationships in Southern Great Plains winter wheat, Agric. For. Meteorol., 184, 48–55, doi:10.1016/j.agrformet.2013.06.007, 2014.

Bloem, E., Haneklaus, S., Kesselmeier, J. and Schnug, E.: Sulfur fertilization and fungal infections affect the exchange of H 2S and COS from agricultural crops, J. Agric. Food Chem., 60(31), 7588–7596, doi:10.1021/jf301912h, 2012.

Blonquist, J. M., Montzka, S. A., Munger, J. W., Yakir, D., Desai, A. R., Dragoni, D., Griffis, T. J., Monson, R. K., Scott, R. L. and Bowling, D. R.: The potential of carbonyl sulfide as a proxy for gross primary production at flux tower sites, J. Geophys. Res. Biogeosciences, 116(4), 1–18, doi:10.1029/2011JG001723, 2011.

Campbell, J. E., Berry, J., Seibt, U., Smith, S., Nature, S. M.- and 2017, U.: Large historical growth in global terrestrial gross primary production, nature.com, 544(7468), 84 [online] Available from: https://www.nature.com/articles/nature22030 (Accessed 29 January 2018a), 2017.

Campbell, J. E., Whelan, M. E., Berry, J. A., Hilton, T. W., Zumkehr, A., Stinecipher, J., Lu, Y., Kornfeld, A., Seibt, U., Dawson, T. E., Montzka, S. A., Baker, I. T., Kulkarni, S., Wang, Y., Herndon, S. C., Zahniser, M. S., Commane, R. and Loik, M. E.: Plant Uptake of Atmospheric Carbonyl Sulfide in Coast Redwood Forests, J. Geophys. Res. Biogeosciences, 122(12), 3391–3404, doi:10.1002/2016JG003703, 2017b.

Cheng, S. J., Bohrer, G., Steiner, A. L., Hollinger, D. Y., Suyker, A., Phillips, R. P. and Nadelhoffer, K. J.: Variations in the influence of diffuse light on gross primary productivity in temperate ecosystems, Agric. For. Meteorol., 201, 98–110, doi:10.1016/j.agrformet.2014.11.002, 2015.

Commane, R., Meredith, L. K., Baker, I. T., Berry, J. A., Munger, J. W., Montzka, S. A., Templer, P. H., Juice, S. M., Zahniser, M. S. and Wofsy, S. C.: Seasonal fluxes of carbonyl sulfide in a midlatitude forest, Proc. Natl. Acad. Sci., 112(46), 14162–14167, doi:10.1073/pnas.1504131112, 2015.

Dalton, M. M., Dello, K. D., Hawkins, L., Mote, P. W. and Rupp, D. E.: The third

539 Oregon climate assessment report, Oregon Clim. Chang. Res. Institute, Coll. Earth,
540 Ocean Atmos. Sci. Oregon State Univ. Corvallis, OR, 2017.

541 Eastman, P. A. K. and Camm, E. L.: Regulation of photosynthesis in interior spruce
542 during water stress: changes in gas exchange and chlorophyll fluorescence, Tree Physiol.,
543 15(4), 229–235 [online] Available from: http://dx.doi.org/10.1093/treephys/15.4.229,
544 1995.

545 Falk, M., Wharton, S., Schroeder, M., Ustin, S. L. and Paw U, K. T.: Flux partitioning in
546 an old-growth forest: seasonal and interannual dynamics, Tree Physiol., 28(4), 509–520,
547 doi:10.1093/treephys/28.4.509, 2008.

548 Gimeno, T. E., Ogée, J., Royles, J., Gibon, Y., West, J. B., Burlett, R., Jones, S. P.,
549 Sauze, J., Wohl, S., Benard, C., Genty, B. and Wingate, L.: Bryophyte gas-exchange
550 dynamics along varying hydration status reveal a significant carbonyl sulphide (COS)
551 sink in the dark and COS source in the light, New Phytol., 215(3), 965–976,
552 doi:10.1111/nph.14584, 2017.

553 Hilton, T., Whelan, M., Zumkehr, A., … S. K.-N. C. and 2017, U.: Peak growing season
554 gross uptake of carbon in North America is largest in the Midwest USA, nature.com,
555 7(6), 450 [online] Available from: https://www.nature.com/articles/nclimate3272
556 (Accessed 29 January 2018), 2017.

557 Hollinger, A. D. Y., Kelliher, F. M., Byers, J. N., Hunt, J. E., Mcseveny, T. M., Weir, L.,
558 Ecology, S. and Jan, N.: Carbon Dioxide Exchange between an Undisturbed Old-Growth
559 Temperate Forest and the Atmosphere Published by : Wiley Stable URL :
560 http://www.jstor.org/stable/1939390 REFERENCES Linked references are available on
561 JSTOR for this article : You may need to log , , 75(1), 134–150, 2017.

562 Johnson, J. E., Bandy, A. R., Thornton, D. C. and Bates, T. S.: Measurements of
563 atmospheric carbonyl sulfide during the NASA Chemical Instrumentation Test and
564 Evaluation project: Implications for the global COS budget, J. Geophys. Res., 98(D12),
565 23443, doi:10.1029/92JD01911, 1993.

566 Kim, Y., Still, C. J., Hanson, C. V., Kwon, H., Greer, B. T. and Law, B. E.: Canopy skin
567 temperature variations in relation to climate, soil temperature, and carbon flux at a
568 ponderosa pine forest in central Oregon, Agric. For. Meteorol., 226–227, 161–173,
569 doi:10.1016/j.agrformet.2016.06.001, 2016.

570 Kitz, F., Gerdel, K., Hammerle, A., Laterza, T., Spielmann, F. M. and Wohlfahrt, G.: In
571 situ soil COS exchange of a temperate mountain grassland under simulated drought,
572 Oecologia, 183(3), 851–860, doi:10.1007/s00442-016-3805-0, 2017.

573 Kooijmans, L. M. J. J., Maseyk, K., Seibt, U., Sun, W., Vesala, T., Mammarella, I.,
574 Kolari, P., Aalto, J., Franchin, A., Vecchi, R., Valli, G. and Chen, H.: Canopy uptake
575 dominates nighttime carbonyl sulfide fluxes in a boreal forest, Atmos. Chem. Phys.,
576 17(18), 11453–11465, doi:10.5194/acp-17-11453-2017, 2017.

577 Launois, T., Peylin, P., Belviso, S. and Poulter, B.: A new model of the global
578 biogeochemical cycle of carbonyl sulfide - Part 2: Use of carbonyl sulfide to constrain
579 gross primary productivity in current vegetation models, Atmos. Chem. Phys., 15(16),
580 9285–9312, doi:10.5194/acp-15-9285-2015, 2015.

581 Maseyk, K., Berry, J. A., Billesbach, D., Campbell, J. E., Torn, M. S., Zahniser, M. and
582 Seibt, U.: Sources and sinks of carbonyl sulfide in an agricultural field in the Southern
583 Great Plains, Proc. Natl. Acad. Sci., 111(25), 9064–9069, doi:10.1073/pnas.1319132111,
584 2014.

585 Notholt, J., Kuang, Z., Rinsland, C. P., Toon, G. C., Rex, M., Jones, N., Albrecht, T.,
586 Deckelmann, H., Krieg, J. and Weinzierl, C.: Enhanced upper tropical tropospheric COS:
587 Impact on the stratospheric aerosol layer, Science (80-.)., 300(5617), 307–310, 2003.

588 Parker, G. G., Harmon, M. E., Lefsky, M. A., Chen, J., Pelt, R. Van, Weis, S. B.,
589 Thomas, S. C., Winner, W. E., Shaw, D. C. and Frankling, J. F.: Three-dimensional
590 Structure of an Old-growth Pseudotsuga-Tsuga Canopy and Its Implications for Radiation
591 Balance, Microclimate, and Gas Exchange, Ecosystems, 7(5), 440–453,
592 doi:10.1007/s10021-004-0136-5, 2004.

593 Paw U, K. T., Falk, M., Suchanek, T. H., Ustin, S. L., Chen, J., Park, Y.-S., Winner, W.
594 E., Thomas, S. C., Hsiao, T. C., Shaw, R. H., King, T. S., Pyles, R. D., Schroeder, M. and
595 Matista, A. A.: Carbon Dioxide Exchange between an Old-Growth Forest and the
596 Atmosphere, Ecosystems, 7(5), 513–524, doi:10.1007/s10021-004-0141-8, 2004.

597 Protoschill-Krebs, G Wilhelm, C Kesselmeier, J.: Consumption of carbonyl sulphide
598 (COS) by higher plant carbonic anhydrase (CA), Atmos. Environ., 30(18), 3151–3156
599 [online] Available from:
600 https://www.sciencedirect.com/science/article/pii/135223109600026X (Accessed 29
601 January 2018), 1996.

602 Protoschill-Krebs, G. and Kesselmeier, J.: Enzymatic pathways for the consumption of
603 carbonyl sulphide (COS) by higher plants, Bot. Acta, 105, 206–212 [online] Available
604 from: http://onlinelibrary.wiley.com/doi/10.1111/j.1438-8677.1992.tb00288.x/full
605 (Accessed 29 January 2018), 1992.

606 Reichstein, M., Falge, E., Baldocchi, D., Papale, D., Aubinet, M., Berbigier, P.,
607 Bernhofer, C., Buchmann, N., Gilmanov, T. and Granier, A.: On the separation of net
608 ecosystem exchange into assimilation and ecosystem respiration: review and improved
609 algorithm, Glob. Chang. Biol., 11(9), 1424–1439, 2005.

610 Sandoval-Soto, L., Stanimirov, M., von Hobe, M., Schmitt, V., Valdes, J., Wild, A. and
611 Kesselmeier, J.: Global uptake of carbonyl sulfide (COS) by terrestrial vegetation:
612 Estimates corrected by deposition velocities normalized to the uptake of carbon dioxide
613 (CO₂), Biogeosciences Discuss., 2(1), 183–201,
614 doi:10.5194/bgd-2-183-2005, 2005.

615 Seibt, U., Kesselmeier, J., Sandoval-Soto, L., Kuhn, U. and Berry, J. A.: A kinetic

616 analysis of leaf uptake of COS and its relation to transpiration, photosynthesis and carbon
617 isotope fractionation, Biogeosciences, 7(1), 333–341, doi:10.5194/bg-7-333-2010, 2010.

618 Shaw, D., Franklin, J., Bible, K., Klopatek, J., Freeman, E., Greene, S. and Parker, G.:
619 Ecological Setting of the Wind River Old-growth Forest, Ecosystems, 7(5), 427–439,
620 doi:10.1007/s10021-004-0135-6, 2004.

621 Stimler, K., Nelson, D. and Yakir, D.: High precision measurements of atmospheric
622 concentrations and plant exchange rates of carbonyl sulfide using mid-IR quantum
623 cascade laser, Glob. Chang. Biol., 16(9), 2496–2503, doi:10.1111/j.1365-
624 2486.2009.02088.x, 2010a.

625 Stimler, K., Montzka, S. A., Berry, J. A., Rudich, Y. and Yakir, D.: Relationships
626 between carbonyl sulfide (COS) and CO2 during leaf gas exchange, New Phytol., 186(4),
627 869–878, doi:10.1111/j.1469-8137.2010.03218.x, 2010b.

628 Sun, W., Maseyk, K., Lett, C. and Seibt, U.: Litter dominates surface fluxes of carbonyl
629 sulfide in a Californian oak woodland, J. Geophys. Res. G Biogeosciences, 121(2), 438–
630 450, doi:10.1002/2015JG003149, 2016.

631 Urban, O., Janouš, D., Acosta, M., Czerný, R., Marková, I., Navrátil, M., Pavelka, M.,
632 Pokorný, R., Šprtová, M., Zhang, R., Špunda, V. R., Grace, J. and Marek, M. V.:
633 Ecophysiological controls over the net ecosystem exchange of mountain spruce stand.
634 Comparison of the response in direct vs. diffuse solar radiation, Glob. Chang. Biol.,
635 13(1), 157–168, doi:10.1111/j.1365-2486.2006.01265.x, 2007.

636 Wehr, R., Commane, R., Munger, J. W., Barry Mcmanus, J., Nelson, D. D., Zahniser, M.
637 S., Saleska, S. R. and Wofsy, S. C.: Dynamics of canopy stomatal conductance,
638 transpiration, and evaporation in a temperate deciduous forest, validated by carbonyl
639 sulfide uptake, Biogeosciences, 14(2), 389–401, doi:10.5194/bg-14-389-2017, 2017.

640 Wharton, S. and Falk, M.: Climate indices strongly influence old-growth forest carbon
641 exchange, Environ. Res. Lett., 11(4), 1–11, doi:10.1088/1748-9326/11/4/044016, 2016.

642 Wharton, S., Falk, M., Bible, K., Schroeder, M. and Paw U, K. T.: Old-growth CO 2 flux
643 measurements reveal high sensitivity to climate anomalies across seasonal, annual and
644 decadal time scales, Agric. For. Meteorol., 161, 1–14,
645 doi:10.1016/j.agrformet.2012.03.007, 2012.

646 Whelan, M. E., Hilton, T. W., Berry, J. A., Berkelhammer, M., Desai, A. R. and
647 Campbell, J. E.: Carbonyl sulfide exchange in soils for better estimates of ecosystem
648 carbon uptake, Atmos. Chem. Phys., 16(6), 3711–3726, 2016.

649 Whelan, M. E., Lennartz, S. T., Gimeno, T. E., Wehr, R., Wohlfahrt, G., Wang, Y.,
650 Kooijmans, L. M. J., Hilton, T. W., Belviso, S., Peylin, P., Commane, R., Sun, W., Chen,
651 H., Kuai, L., Mammarella, I., Maseyk, K., Berkelhammer, M., Li, K.-F., Yakir, D.,
652 Zumkehr, A., Katayama, Y., Ogée, J., Spielmann, F. M., Kitz, F., Rastogi, B.,
653 Kesselmeier, J., Marshall, J., Erkkilä, K.-M., Wingate, L., Meredith, L. K., He, W., Bunk,

R., Launois, T., Vesala, T., Schmidt, J. A., Fichot, C. G., Seibt, U., Saleska, S., Saltzman, E. S., Montzka, S. A., Berry, J. A. and Campbell, J. E.: Reviews and Syntheses: Carbonyl Sulfide as a Multi-scale Tracer for Carbon and Water Cycles, Biogeosciences Discuss., (October), 1–97, doi:10.5194/bg-2017-427, 2017.

Winner, W., Thomas, S., Berry, J., Bond, B., Cooper, C., Hinckley, T., Ehleringer, J., Fessenden, J., Lamb, B., McCarthy, S., McDowell, N., Phillips, N. and Williams, M.: Canopy Carbon Gain and Water Use: Analysis of Old-growth Conifers in the Pacific Northwest, Ecosystems, 7(5), 482–497, doi:10.1007/s10021-004-0139-2, 2004.

Wohlfahrt, G., Brilli, F., Hörtnagl, L., Xu, X., Bingemer, H., Hansel, A. and Loreto, F.: Carbonyl sulfide (COS) as a tracer for canopy photosynthesis, transpiration and stomatal conductance: Potential and limitations, Plant, Cell Environ., 35(4), 657–667, doi:10.1111/j.1365-3040.2011.02451.x, 2012.

Woodruff, D. R., Mcculloh, K. A., Warren, J. M., Meinzer, F. C. and Lachenbruch, B.: Impacts of tree height on leaf hydraulic architecture and stomatal control in Douglas-fir, Plant, Cell Environ., 30(5), 559–569, doi:10.1111/j.1365-3040.2007.01652.x, 2007.